Chapter 5

Course Analysis

"Optimal results" from feedback-loop experiments usually represent the last iteration; this chapter tries to demonstrate that there is more information to extract from an OCE than just one solution. The "course-analysis" procedure for optimal search, introduced in this chapter, will analyze two coherent control experiments; one will be the ionization of the NaK molecule, and the other isotope ratio optimization of K_2^+.

5.1 Introduction

There are many ways adapting a search strategy to a particular goal in order to improve performance, reliability, and solution quality. Nevertheless, the "No-Free-Lunch-Theorem" declares that every imaginable search algorithm (even random search) performs equally when averaged over all possible problems [74]. Improving search speed and (very important for coherent control) simplicity are still valid goals that can be pursued to understand more about the examined quantum systems. One can classify two approaches of improving and adapting algorithms, one is at run-time and the other afterwards.

An example for the first approach are tailored cost functionals for the fitness function, as discussed in the previous chapter. Non-traditional operators such as phase smoothing, time-domain crossover, and polynomial phase mutation were incorporated by the group of Bucksbaum in order to enable new search paths (through time-domain crossover) and remove excessive temporal structures (with the phase smoothing operator). The question of the influence of the new operators was treated with a self-adaptive approach and operator use itself became subject of evolution [93, 94]. For the second approach, there exist a few methods of analyzing the accumulated genetic data, for example, calculating nonlinear functional maps [95] or experimental search space maps [96, 97]. Another interesting tool is principal component analysis (PCA), which allowed to uncover the degrees of freedom in the control Hamiltonian for stimulated Raman scattering in liquid methanol [98].

In this chapter, a similar technique will be presented, as the progress of an OCE is analyzed, but unlike PCA, no abstract degrees of freedom are to be uncovered, but physical meaningful and intuitive parameters, for example sub pulses in time and spectral features.

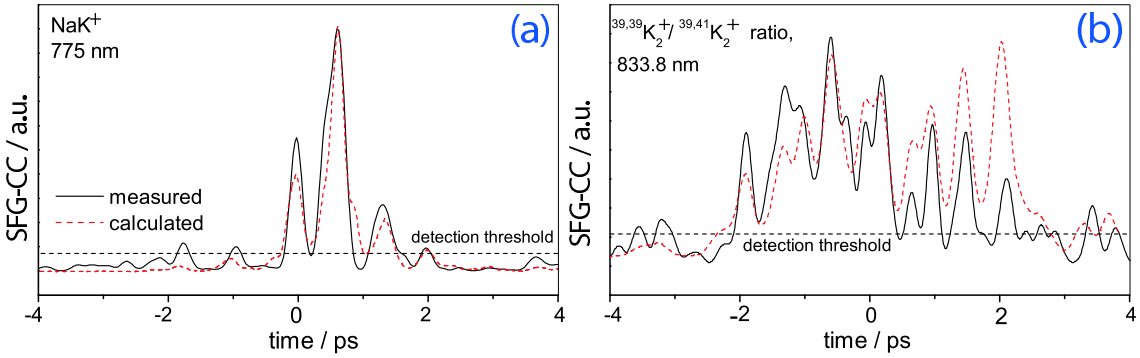

Figure 5.1: Accuracy estimate for the calculation of a pulse form from recorded phase- or transmission patterns. Graph (a) shows the measured SFG-CCs of an NaK ionization optimization and (b) a $^{39,39}K_2/^{39,41}K_2$ ion ratio optimization. A peak detection threshold reduces the number of peaks to be tracked during the analysis.

5.2 Pulse reconstruction

If T_i and ϕ_i are stored for every individual for every generation, an analysis can be performed after an experiment, and one is free to choose which features are studied. As it would be quite time-consuming to experimentally acquire hundreds of SFG-CC traces that demand scanning a delay stage[1], the pulses will be calculated from the transmission and applied phase, which constitute the complex spectral filter $\tilde{H}(\omega)$, using the formalism described in Sections 2.2 and 3.4.

The obtained SFG-CCs match the measured cross-correlations quite passably, which is pictured in Fig. 5.1. There is a very good agreement when only few sub pulses are involved, as shown in the result for the NaK molecule (a); for phase patterns that have a higher complexity like the K_2 case (b), a qualitative agreement is reached, with an average error of ± 8 fs for the peak positions in time. The deviations originate from the issues described in Section 2.2 and probably a small misalignment. To visualize the tracking process, an intensity threshold that is dynamically adapted to the total pulse energy is introduced (the dashed line in the figures) in order to let only the most prominent sub pulses leave a trail.

5.3 NaK course analysis

The experiments analyzed in this chapter were carried out with the 80 MHz system at a central wavelength of 775 nm and a bandwidth of 8 nm, using the SLM-256 in phase-only mode.

The pulse from the last iteration of the NaK phase-only ionization maximization experiment[2], shown in Fig. 5.1 (a), can be explained by a first excited $A(2)^1\Sigma^+$ state wavepacket [22, 23]. After 1.5 periods, which is close to the measured distance of 680 fs, the next sub pulse occurs, and via a two-photonic transition, transfers population to the detectable ionic state, but also simultaneously excites more population from

[1] Other characterization techniques, like SPIDER [99] or SHG-FROG [35] are of course faster, but require a pulse retrieval.

[2] also presented in another context (central frequency-dependent optimization) in Ref. [77]

the ground to the first excited stated. The last sub pulse (arriving after 690 fs) again transfers population to the ionic state with a total optimization factor of 1.6 compared to an unshaped pulse.

5.3.1 Tracking an NaK optimization

The accumulated genetic data will be used to track the ion yield, the number of sub pulses above threshold, the sub pulse position in time, their distance, and intensity, which is visualized with a scatter graph of the respective values versus iteration in Fig. 5.2.

The course of the ion yield, plotted in (a), of the best, mean, and worst individual is increasing steadily until, from generation 89 on, no significant increase in ion signal is observed, and the experiment is terminated manually at generation 146. When looking more closely, "plateaus", where the ion signal stays relatively constant, and "transition periods" can be made out, which are indicated by the vertical lines. The steady phases can be explained by the elitism of the algorithm which carries the best individual to the next generation where it will be measured again, if no competitor takes its place, or is killed by experimental noise that reduced its fitness and/or simultaneously has increased the fitness of an inferior rival. It is interesting to note that the final number of prominent sub pulses (b) is reached by a more or less steady decrease till generation 89, where the number drops to the final value. From this generation on, no more increase in ion yield occurs.

Graph (c) depicts the development of the sub pulse's absolute position in time (the peak intensities are encoded in the gray level, which are darker, when more intense), which, at a first glance, is suspiciously steady. It is interesting that an "absolute temporal" position can be observed, as for a molecule travelling through the focal zone of a femtosecond pulse train, a temporal waveform shift of femto- or picoseconds is not supposed to provide a different ion yield. The establishment of absolute temporal positions could be determined to originate from the pulse encoding and the circumstances of the shaper setup. As the linear Taylor term b_1 in Eq. 2.24 corresponds to an absolute shift of a pulse envelope in time, a time shift of the whole pulse train would require an distinct effort of mutation and crossover, involving all pixels as a linear spectral phase component would have to be changed throughout the whole array. The available shaping window (which corresponds to the intensity distribution one single transmitting pixel would yield in time [36, 100]) also has a distinct influence. The maximum intensity at a point in time is determined by this window, which is maximal at t=0 (defined by a pulse having a flat phase) and therefore, for Fourier shaping, a coupling of shaping window and maximal intensity in time is the result. For the employed encoding and similar experiments, it can be assumed that first, the most important pulses are anchored in time before continuing to the remaining ones. This behavior also allows to track sub pulses and trace a "distance", like the main pulse (+640 fs absolute) and the second most intense (at -40 fs).

In (d), the temporal distances between the sub pulses are displayed, having the issue, that sometimes, newly arising pulses split the distances between two previously existing pulses. The gray level of the points is encoded as $\sqrt{I_1 \cdot I_2}$ using the respective two sub pulse's intensities. Graph (e) finally displays the course of the

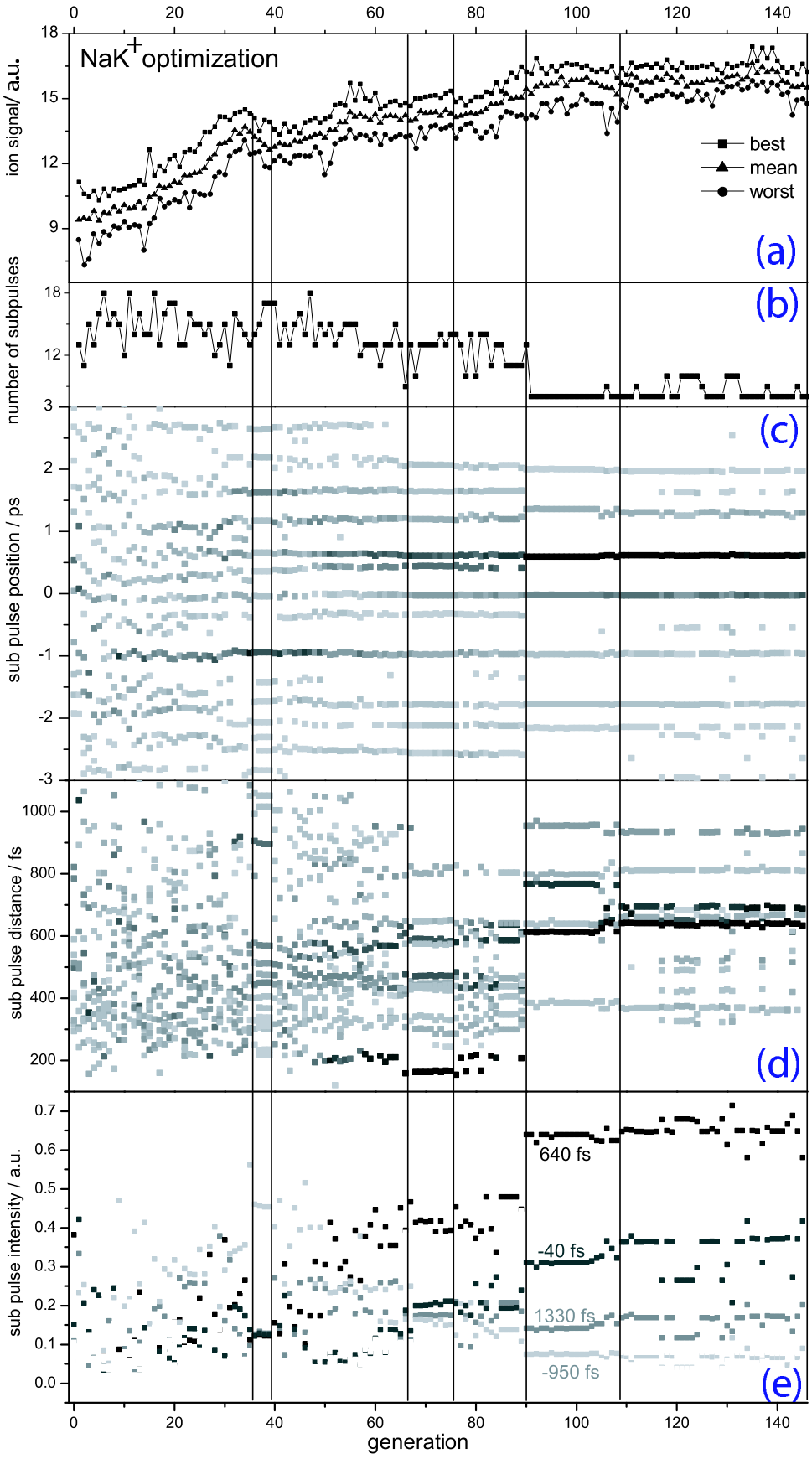

Figure 5.2: Course analysis of the maximization of the NaK ion yield: (a) ion yield, (b) number of sub pulses, (c) sub pulse positions, (d) sub pulse distances, and (e) sub pulse intensities.

temporal sub pulse intensities, with a gray scale according to their temporal position.

In a survey, until generaton 35, chaotic behavior can be seen for all the plots, which also corresponds to the first rise of the ion signal. From the beginning to generation 67, many feature rearrangements take place, producing a steady rise of ion yield. In the following, stationary period (until generation 76), for the first time, the pulse distances are steady for a while, meaning that a local optimum is probed. The final rise (generations 77-90) brings a drastic reduction of the number of pulses above threshold and due to the conservation of pulse energy for phase-only shaping, a concentration of pulse energy to a few major sub pulses occurs, which then dominates the wavepacket propagation that takes place. After that, the final ion yield is reached, and as far as the experimental noise admits, no further development would be expected. But there is still a slight adaptation of the sub pulse's peak intensities, which can be seen in the changing gray values in (c), and from the peak intensity course (e) which would go unnoticed without a course analysis. This implies that there is still energy redistribution at work, allowing to estimate how representative the solution from the last generation will be. Apparently, the fine-tuning of temporal sub pulse intensities has no particular influence on the ion yield, which can be interpreted in a way that its importance is somewhat inferior, and a proper wavepacket localization on the energy surfaces is more important than an as-precise-as-possible sub pulse intensity relation.

Recapitulating, the observation can be made that first, the rough pulse positions, then their distances, and later on their intensities are adjusted by the algorithm.

5.4 K_2 course analysis

The next course analysis covers an optimal control experiment that features isotope selective ionization of the potassium molecule with optimally shaped pulses [89, 101], also described in detail in Ref. [55].

Isotope separation is usually performed by gaseous diffusion or centrifugation [102], laser based isotope separation [103, 104] takes advantage of small isotope shifts in the spectral lines, but needs tuneable, narrowband radiation and, unfortunately, a quite elaborate spectroscopic knowledge of the system. Separating isotopes using wavepackets exploits differences in the wavepacket dynamics of the isotopes, or alternatively, continuous pump-dump processes [105, 106]. Here, a femtosecond pulse train will be utilized in order to irradiate both $^{39,39}K_2$ and $^{39,41}K_2$ isotopes in the gas phase; and the method of control will be phase- and amplitude modulation. The isotope's ion signal was sequentially recorded by the quadrupole mass spectrometer, with a higher noise level, caused by the division of two signals. The read-out requires a constant switching of the extraction voltages and a triggered recording procedure with no room for erroneous data points [71, 101].

The electronically excited states (see Fig. 5.3) of K_2 have already been investigated by means of femtosecond pump-probe spectroscopy, where an oscillation period of 500 fs on the $A^1\Sigma^+$ state could be established.

Despite having very similar molecular potentials, $^{39,39}K_2$ and $^{39,41}K_2$ exhibit a fundamentally different long-term behavior in pump-probe experiments [56, 108] (see Fig. 5.4).

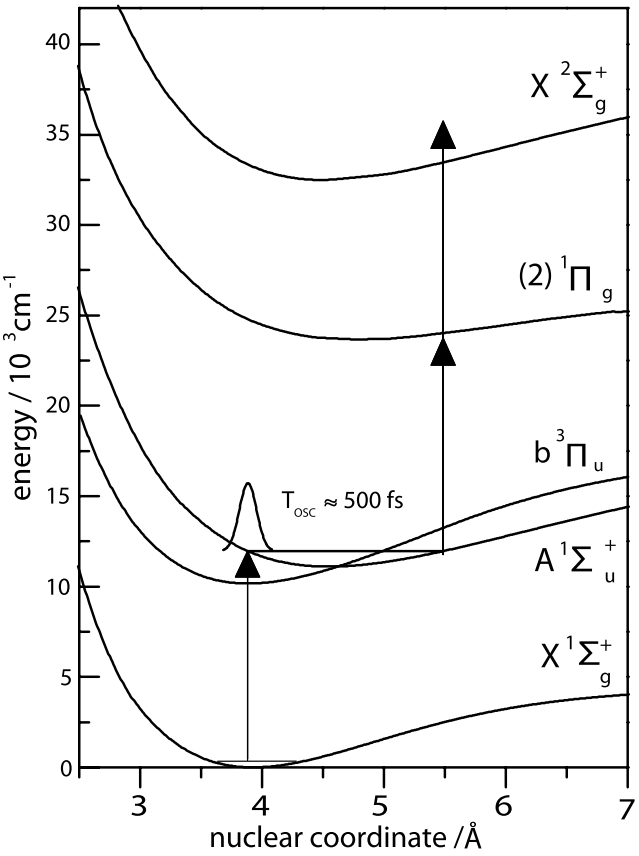

Figure 5.3: Potential energy scheme for the potassium molecule, taken from [101].

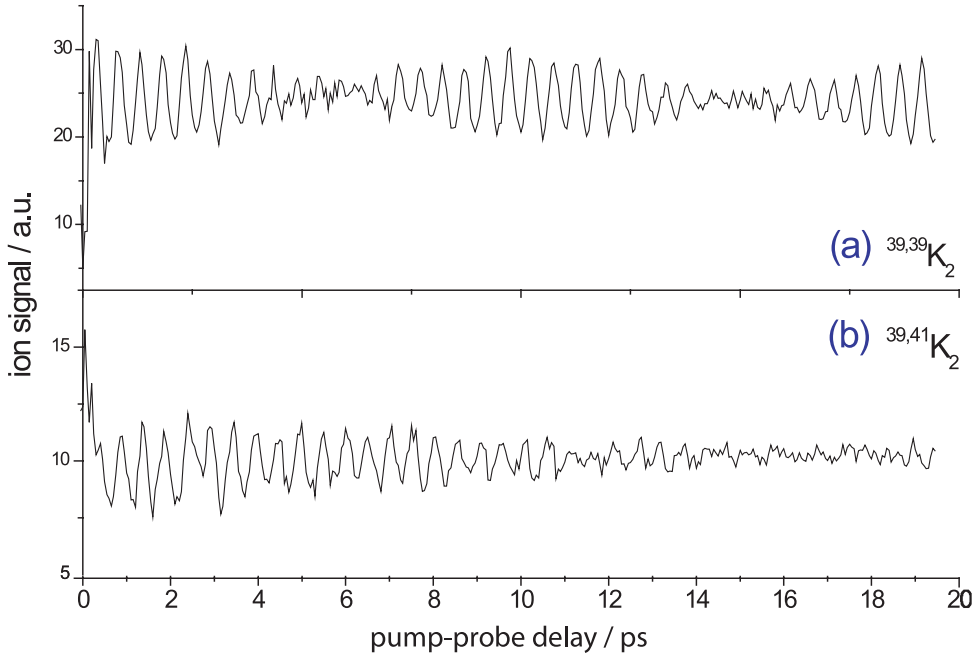

Figure 5.4: Comparison of the long-term wavepacket behavior for two isotopes of K_2 due to different perturbations of the $A^1\Sigma_u^+$ state by the crossing $b^3\Pi_u$ triplet state. For $^{39,39}K_2$ (a), a beat signal is observed, for the $^{39,41}K_2$ isotope, dephasing of the wavepacket occurs with fractional revivals [107] (taken from Ref. [55]).

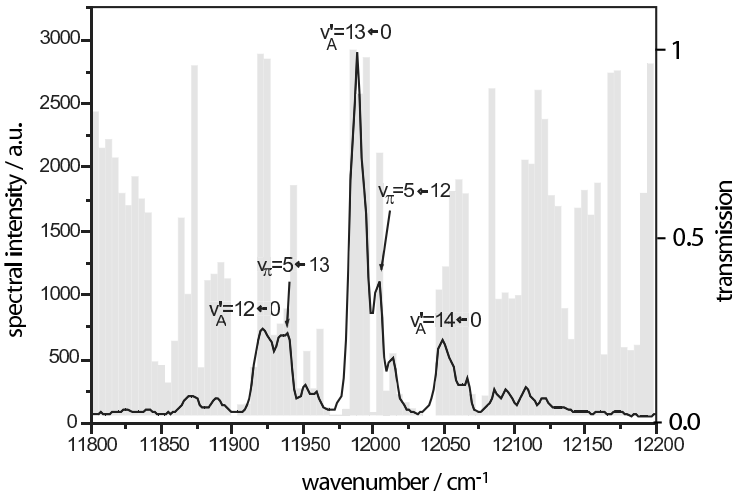

Figure 5.5: Pulse spectrum for a maximization of the $^{39,39}K_2/^{39,41}K_2$ isotope ratio with phase and amplitude modulation, obtaining a factor of 72:1; the gray bars are the pixel transmissions. Taken from Ref. [89].

For $^{39,39}K_2$, spin-orbit interaction effects enable an intersystem crossing between the two potential energy surfaces $A^1\Sigma_u^+$ and $b^3\Pi_u$, which leads to a shift of the $v'_A = 12, 13$ vibrational levels of 1.2 cm^{-1} and 2.1 cm^{-1} [109, 108]. For the $^{39,41}K_2$ isotope, a dephasing is observed, while a recurrence from 5 ps on can be seen for $^{39,39}K_2$.

The best isotope selectivity for maximization of the $^{39,39}K_2$ / $^{39,41}K_2$ isotope ratio can be obtained if the $^{39,39}K_2$ transition states can be populated as highly as possible while, simultaneously, a population of the $^{39,41}K_2$ states can be avoided by an assortment of frequencies within the broadband spectrum, with an additional contribution of usually quite complex wavepacket dynamics, induced by a multitude of sub pulses.

The spectral peaks from the final generation could be assigned to vibrational levels in the electronic transitions $A^1\Sigma_u^+ \leftarrow X^1\Sigma_g^+$ and $2^1\Pi_g \leftarrow A^1\Sigma_u^+$ [89]. The optimized pulses feature very sharp frequency patterns - see Fig. 5.5 - and a complex temporal structure. The combined spectral and temporal shaping effort lead to a wavepacket propagation caused by the optimized pulse, which resulted in a significant enhancement of the ionization efficiency of one isotope compared to the other (from an original 6.8:1 $^{39,39}K_2$:$^{39,41}K_2$-ratio to 72:1 for the optimized pulse).

Fig. 5.5 shows the spectral result of a K_2 isotope ratio maximization experiment where several peaks could be assigned to vibrational levels to the electronic transitions $A^1\Sigma_u^+ \leftarrow X^1\Sigma_g^+$ and $2^1\Pi_g \leftarrow A^1\Sigma_u^+$.

5.4.1 Tracking a K_2 optimization

Temporal course. In Fig. 5.6, the course of the algorithm that provided a factor of 72:1 for $^{39,39}K_2$:$^{39,41}K_2$ is plotted, whereby (a) displays the derived fitness (isotope ion ratio), (b) the number of sub pulses, (c) the absolute sub pulse position in time, (d) the pulse distances, and (e) the zero order phase b_0 at the peak position. The most obvious difference to Fig. 5.2 is that there is no plateau-like behavior, but an overally continuous rise until generation 189 where the final ratio is reached. The convergence time is also twice as long compared to NaK because of the higher problem complexity. During the whole run the number of sub pulses above the dynamically adapted detection threshold stayed more or less constant at 12. There was also an additional 50 % decline of total power during the run due to amplitude modulation. From an overview, one can make out a chaotic period which lasts until generation 126 (first vertical line from the left); from then on, an agglomeration of sub pulse distances (d) and phases (e) can be observed. The issue of reliability of the "final" pulse can be addressed when looking at the significant accumulation of pulse distances (d) to 250 fs and 500 fs, which is T_{osc} and $0.5 \cdot T_{osc}$ of the first excited $A^1\Sigma_u^+$ state. This is also illustrated by the small histogram at the right edge of (d), which superposes the last 130 generations. Another remarkable issue is the aggregation of phases (e) from generation 80 on; and about four discrete levels can be made out after generation 126. While not claiming quantitative readings because of the indirect method of determining this observable (and no phase measurement with adequate equipment like SPIDER [99] was performed), this qualitative feature is good enough to support an explanation of a stepwise excitation with constructive and destructive interferences at the inner and outer turning point[3]. This result can be regarded as a further step in understanding such complicated twelve-sub pulse structures. Recently, a joint theory-experimental effort [110] on isotope selection of the fellow alkali dimer NaK substantiated the importance of phases in such isotope selective processes[4].

Spectral course. There is more information available when amplitude modulation is enabled as spectral features are also bound to evolve. In Fig. 5.7 (a) peaks in the spectrum are tracked (leading to Fig. 5.5, the final result). The optimization starts, as always, with a random pattern; differently than the temporal features, spectral characteristics develop within the first 10 generations and after that, only a few of these peaks "die out"; and there is no more pronounced change in the peak's wavelengths. As an obvious, secondary feature, the peak's intensities develop slower - see (b) - and there is still redistribution between the peaks until generation 189, where the color scale that is encoded in wavelengths assists in tracking the single peaks during the run.

The peaks that are eliminated during the run can also provide additional information. One can read from Fig. 5.7 that spectral lines close to $2^1\Pi_g \leftarrow A^1\Sigma_u^+$ transitions at 836.8 nm ($v = 5 \leftarrow v' = 13$) and 830.2 nm ($v = 8 \leftarrow v' = 14$) of $^{39,41}K_2$ are eliminated during the experiment. It is reasonable to conclude that the

[3] which is further backed up by the fact that the Franck-Condon window (via the resonant $2^1\Pi_g^+$ state) is favorable at these nuclear distances

[4] see also Ref. [111, 112]

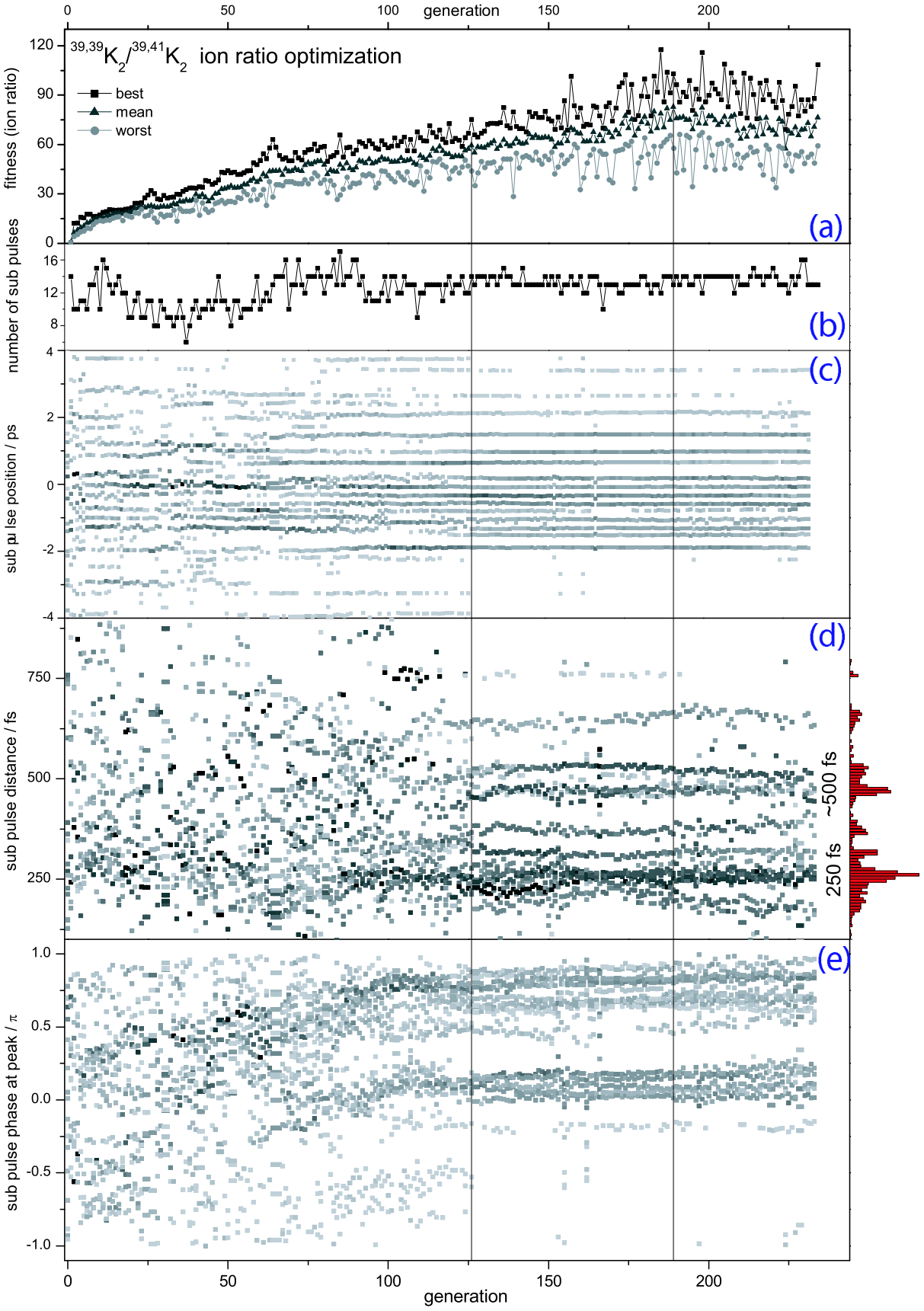

Figure 5.6: Course analysis of K_2 isotope selective ionization.

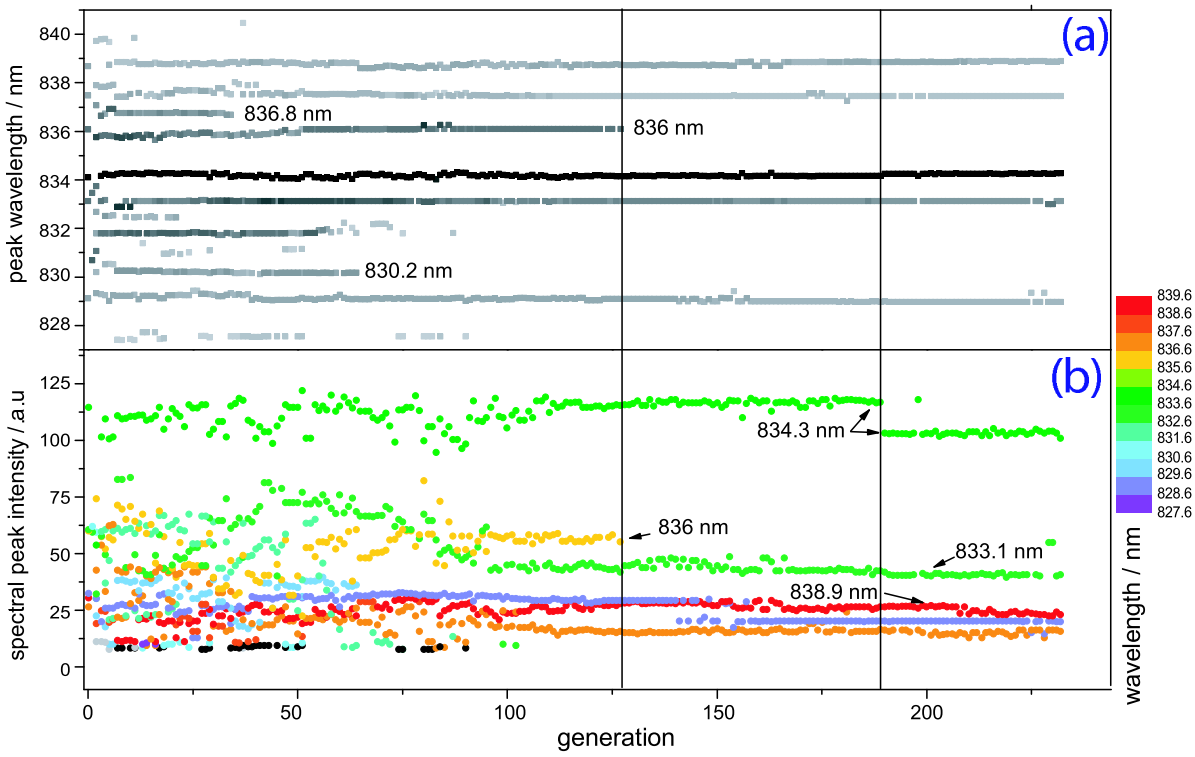

Figure 5.7: Spectral course of the K_2 ratio ion optimization. (a) Wavelength of identified spectral peaks versus generation, (b) intensity course of the peaks, which can be tracked using the color scale on the right.

removal of these frequencies circumvents ionization of the $^{39,41}K_2$ population already being present in the $A^1\Sigma_u^+$ state with the result that the overall isotope selectivity is improved.

For determining the "importance" of spectral versus time domain, a cause-and-effect behavior can be found when looking at the evolution of the spectral peak at 836 nm in Fig. 5.5 (b). When this peak dies out at generation 126, a significant restructuring of the temporal features towards the final solution takes place (marked also by one of the vertical lines in Fig. 5.6). Convergence to the final solution is later "announced" when the 834.3 nm peak drops in intensity by 12 % at generation 189 (see arrows). These two occurrences mark quite interesting events, and it could be a good idea to perform additional experimental snapshots on such occasions, provided that the features are monitored in real-time.

Overally, an order of convergence for the depicted features can be provided: First, the spectral peak positions converge while their intensities are still being determined. The temporal features approach their final value much slower with a great deal of rearranging, caused by certain spectral events. The higher importance of the spectral domain also agrees with amplitude-only measurements [89] where a total optimization factor (maximization÷minimization) of 40 was obtained whereby phase-only provided only a factor of 2; whereby combined phase and amplitude yielded a total optimization factor of 140.

5.5 Conclusion and Outlook

This chapter tried to give a tour through the search spaces of two very different optimal control experiments. Features that can be easily spotted and measured were selected, for example pulse distances and spectral peaks, but also indirect properties such as the phases at peak. This approach is not intended to reveal hidden search space variables but determines the relationship and evolution of the ones that are selected for study. The goal was to show that there is useful information to extract from the experimental course of an evolutionary algorithm. Observing how, and in which order the algorithm achieves its goal helps assigning priorities of further theoretical or experimental studies in order to obtain information how the induced wavepacket dynamics evolves from the initial to the final quantum state. By means of order of convergence, one can assign parameter importance as experience taught that the more important particular features are, the higher their reproducibility.

There have been several expectations on the results of the analysis, as the optimized pulses were already interpreted before. Some results were, however, quite unexpected, like temporal reorganizations due to small changes in the pulse spectra, and the condensation of the temporal phases to a few values.

In any case, checking how the final result of an optimization is related to the solutions from the iterations immediately before termination, should be a general requirement. Also, other parameters as the above used could be tracked, for example sub pulse's fluences to see if there was a correlation of pulse intensity and e.g. ion yield [76]. Sub pulse phase differences (e.g. to inspect two-photon transition probabilities [59, 113]) could also be tracked, as well as Taylor terms for a chirp analysis. If, after an experimental run, a general overview of the features is calculated, key-events can be documented or inspected more closely under the same experimental conditions. When the parameters are calculated directly from the genome, the analysis could be performed on-the-fly, while an experiment is running. This could help not only of tuning the metaheuristics of the algorithm to a better and more reliable performance, but also assure a reasonable cancellation.

There are still open questions about how the algorithm examines search space or if there is a way of determining its current "focus". Performing a feature analysis combined with pulse cleaning could help gaining insight how and if such a focus changes during a run.

A straightforward way putting the insight from this chapter into use will be "parametric shaping", a re-definition of search space, introduced in the next chapter.